electronics

Article

Cooperative NOMA with RIS Assistance for Short-Packet Communications Under Hardware Impairments †

Wenbin Song, Dechuan Chen *, Jin Li, Xingang Zhang and Zhipeng Wang

School of Physics and Electronic Engineering, Nanyang Normal University, Nanyang 473061, China
* Correspondence: chenchuan927@163.com

† This article is a revised and expanded version of a paper entitled Performance Analysis of RIS-Assisted Cooperative NOMA Systems with Finite Blocklength, which was presented at the Seventeenth International Conference on Wireless Communications and Signal Processing, Chongqing, China, 23–25 October 2025.

Abstract

Ultra-reliable low-latency communication (URLLC) presents significant challenges in simultaneously guaranteeing stringent latency bounds, ultra-high reliability, and efficient resource utilization under dynamic channel conditions. To address these joint constraints, a novel framework that integrates a reconfigurable intelligent surface (RIS) with cooperative non-orthogonal multiple access (NOMA) is proposed for short-packet communications. Two distinct phase configuration designs for the RIS are considered, i.e., a near-user priority strategy (NUPS) and a far-user priority strategy (FUPS). The NUPS configures the RIS to enhance the received signal power for the near user, while the FUPS optimizes the phase shifts to maximize the received power for the far user. Closed-form expressions that characterize the average block error rate (BLER) of the near and far users under the two proposed strategies in the presence of hardware impairments are derived. Specifically, the analysis for the far user considers both selection combining (SC) and maximum ratio combining (MRC) reception schemes. Based on the average BLER, we then derive a closed-form expression for the effective throughput. Simulation findings reveal the following: (1) The far user in the proposed cooperative NOMA achieves a lower average BLER than in the non-cooperative NOMA. (2) When the RIS is deployed in close proximity to the base station (BS), the NUPS can effectively leverage the RIS to enhance the far user's signal quality through cooperation, without sacrificing the near user's priority; and (3) SC serves as a low-complexity alternative that achieves near-optimal performance when inter-user channel conditions are favorable.

Keywords: reconfigurable intelligent surface (RIS); cooperative non-orthogonal multiple access (NOMA); average block error rate (BLER); effective throughput

check for updates

Academic Editor: Hector E. Nistazakis

Received: 10 October 2025
Revised: 3 November 2025
Accepted: 5 November 2025
Published: 6 November 2025

Citation: Song, W.; Chen, D.; Li, J.; Zhang, X.; Wang, Z. Cooperative NOMA with RIS Assistance for Short-Packet Communications Under Hardware Impairments. *Electronics* **2025**, *14*, 4352. https://doi.org/10.3390/electronics14214352

Copyright: © 2025 by the authors. Licensee MDPI, Basel, Switzerland. This article is an open access article distributed under the terms and conditions of the Creative Commons Attribution (CC BY) license (https://creativecommons.org/licenses/by/4.0/).

1. Introduction

The passive reconfigurable intelligent surface (RIS) has recently garnered significant interest in wireless communications due to its potential to provide high data-rate services for next-generation networks in a remarkably cost- and energy-efficient manner [1–3]. Such a passive RIS is a planar structure comprising a large number of passive reflective elements. As a passive device, it operates without power-intensive radio frequency chains. To intelligently reshape the wireless propagation environment, the channel information is first estimated. This information is then converted into control signals for the phase shifts of the RIS, which configures the bias voltages of its tunable elements (e.g., varactor

diodes or positive intrinsic negative (PIN) diodes). By smartly adjusting the phase shifts of all its passive elements, the signals reflected from the RIS can coherently combine at the intended receiver, thereby enhancing communication reliability even in challenging channel conditions [4]. The passive nature of its signal reflection enables flexible deployment on facades or indoor walls, as it does not require a power supply to amplify signals. Although a power supply is needed for the control circuit to reconfigure its elements (e.g., using a microcontroller), the overall power consumption remains exceptionally low. This makes it an energy-saving and cost-effective solution that aligns with green communication objectives. Moreover, the integration of the RIS into current network infrastructures is greatly facilitated, as it requires minimal to no hardware modifications to existing base stations (BSs), access points, or end-user devices [5,6].

Due to superior spectral efficiency and massive connectivity capabilities, non-orthogonal multiple access (NOMA) has also attracted significant attention as a pivotal technique for future wireless networks [7–9]. To enhance the performance of NOMA networks further, a promising development known as cooperative NOMA was introduced by Ding et al. [10]. The fundamental concept behind cooperative NOMA is that users with stronger channel conditions act as relays to assist the transmission to those with poorer channels. In cooperative NOMA networks, a supplementary cooperative transmission link provides spatial diversity alongside the direct link to help combat signal fading and increase the overall coverage area [11]. This improved reliability significantly boosts the communication performance for the weak users. Consequently, cooperative NOMA enhances the fairness of NOMA transmissions, especially in scenarios where the weak user is located at the cell edge [12].

However, the performance of cooperative NOMA is still limited by the uncontrollable wireless propagation environment. To address this, the integration of a RIS offers a promising solution [13]. By optimizing the RIS's reflection coefficients, the channel quality for both the direct and cooperative links can be proactively enhanced. This capability introduces new degrees-of-freedom in the system design, enabling RIS-aided cooperative NOMA networks to achieve superior performance. In particular, Zuo et al. [12] introduced an alternating optimization framework for RIS-assisted cooperative NOMA networks to achieve minimal total transmit power. This method jointly optimizes the active beamforming vectors, power allocated for relaying, and phase shifts of the RIS elements. Building on the work in [12], Elhattab et al. [14] extended it to full-duplex (FD) cooperative NOMA networks. When the cooperation between the strong user and weak user was conducted through a device-to-device (D2D) channel, Gu et al. [15] demonstrated that various degrees of diversity gain are achievable in the proposed cooperative RIS-NOMA network by adjusting the number of RIS elements. Zhang et al. [16] explored the use of simultaneous wireless information and power transfer (SWIPT) in RIS-assisted cooperative NOMA networks and derived closed-form expressions for the outage probability. The joint optimization of beamforming coefficients, power splitting factors, and reflection coefficients was addressed by Ren et al. [17] to maximize the achievable rate for the strong user under a strict quality of service requirement for the weak user. In [18], Muhammad et al. proved that combining RIS with cooperative NOMA significantly reduces information age by optimizing power control and RIS phase shifts. Simultaneously transmitting and reflecting RIS (STAR-RIS) was subsequently incorporated into the framework of cooperative NOMA by Toregozhin et al. [19] to improve spectral and energy efficiency.

The rise of the Internet of Things (IoT) and mission-critical control is driving a critical shift in wireless communication paradigms [20,21]. In contrast to traditional scenarios focused on high throughput, these emerging applications rely on frequent short-packet exchanges [22]. This shift necessitates a fundamental re-evaluation of communication theo-

ries, as the classical Shannon capacity theorem becomes inadequate and even misleading for characterizing performance in this regime. Shannon's theory, which provides the fundamental limits of reliable communication, is an asymptotic result that assumes infinitely long codewords. In the short-packet regime, however, finite blocklength and stringent reliability constraints introduce a significant penalty in coding rate [23]. Therefore, new metrics and analytical frameworks are essential. A key performance measure that has emerged is the maximum achievable coding rate at a finite blocklength and a given decoding error probability [24]. Then, a derivation of the average block error rate (BLER) was presented by Vu et al. [25] for RIS-assisted short-packet NOMA networks, demonstrating significant performance gains over orthogonal multiple access (OMA). The interplay between optimal power allocation and minimum common blocklength was investigated by Yuan et al. [26]. To maximize the overall device throughput, Lou et al. [27] constructed an optimization problem to jointly design the blocklength and phase shifts of RIS. Wang et al. [28] addressed the multi-objective problem of joint throughput maximization and blocklength minimization by converting it into a tractable single-objective problem using the Chebyshev method. Given a certain probability of failure for the reflecting elements, Yang et al. [29] derived asymptotic closed-form expressions for the average BLER of NOMA users.

Notably, a key limitation of the approaches proposed in [25–29] is the assumption of ideal transceiver nodes. This assumption does not hold in practice, as all practical nodes are subject to hardware impairments, such as imperfect radio frequency components and phase noise. Lioce et al. [30] revealed the impact of circuit non-idealities on RIS system-level performance. Specifically, Xia et al. [31] examined the average BLER performance of a RIS-assisted NOMA downlink network with short-packet communications, taking into account transceiver hardware impairments. Ren et al. [32] considered the simultaneous presence of both direct and RIS-reflected links from a BS to a pair of NOMA users and accounted for the effects of hardware impairments. In wireless-powered RIS-assisted cognitive NOMA networks, Kumar et al. [33] analyzed the latency and reliability performance under hardware impairments. Imperfect SIC was considered by Ma et al. [34] for RIS-aided short-packet NOMA networks with hardware impairments. The average BLER of active STAR-RIS-assisted NOMA networks with hardware impairments for the short-packet regime was derived by Kumar et al. [35]. The studies in [31–35] focused on conventional NOMA protocols, in which users decode their signals directly from the superimposed transmission. Although NOMA efficiently serves multiple users simultaneously, the weak user often experiences poor channel conditions, which severely limits its data rate and reliability. This problem becomes particularly critical in short-packet communications for ultra-reliable and low-latency communication (URLLC), where the coding gains of traditional infinite blocklength are absent. Consequently, using NOMA without cooperative assistance often fails to meet the ultra-reliability requirements of critical applications. A theoretical analysis was performed by Zheng et al. [36] for cooperative NOMA networks with RIS assistance under the assumption of ideal hardware. However, cooperative NOMA relies on precise successive interference cancellation (SIC), a process highly sensitive to distortion. Hardware impairments can severely degrade the SIC process, causing error propagation and fundamentally limiting the achievable gain for the weak user. Consequently, there is a critical need to holistically and realistically evaluate the reliability of RIS-assisted cooperative NOMA networks, accounting for the practical constraints imposed by hardware imperfections and short-packet transmission.

Inspired by the above observations, in this work, we investigate reliable transmission in cooperative NOMA networks with RIS assistance over Nakagami-m fading channels. To enhance the transmission reliability of a far user, a cooperative decode-and-forward (DF) strategy is utilized, with a near user acting as an intermediate relay node. Besides, we

consider a more practical assumption of imperfect hardware at all nodes, i.e., transceivers at a BS and both users are all subject to hardware impairments. The main contributions of this paper are summarized as follows:

1. We investigate a downlink cooperative NOMA network that utilizes short-packet communications and is enhanced by a RIS. We examine two distinct RIS phase configuration strategies, i.e., a near-user priority strategy (NUPS) and a far-user priority strategy (FUPS). The NUPS configures the RIS to enhance the received signal power for the near user, while the FUPS optimizes the phase shifts to maximize the received power for the far user.
2. We quantify the average BLER performance for the near and far users under the two proposed strategies through derived closed-form expressions, which incorporate the effects of hardware impairments. Specifically, the reception at the far user is studied for two diversity techniques, that is, selection combining (SC) and maximum ratio combining (MRC). Based on the average BLER, we provide a closed-form expression for the effective throughput of the system.
3. The numerical simulations confirm the accuracy of the theoretical analysis and demonstrate that the proposed cooperative NOMA provides a lower average BLER for the far user than the non-cooperative NOMA. In addition, deploying the RIS in proximity to the BS enables the NUPS to cooperatively enhance the far user's signal quality, without sacrificing the near user's priority. Moreover, under favorable inter-user channel conditions, SC is a low-complexity alternative that achieves near-optimal performance.

Table 1 summarizes the key distinctions between the contributions of this work and those of existing related studies.

Table 1. Comparison of this work with related papers.

	[14]	[15]	[29]	[31]	[32]	[36]	**This Work**
RIS	✓	✓	✓	✓	✓	✓	✓
NOMA	✓	✓	✓	✓	✓	✓	✓
Cooperative transmission	✓	✓				✓	✓
Short-packet communications			✓	✓	✓	✓	✓
Hardware impairments				✓	✓		✓
Average BLER			✓	✓	✓	✓	✓

The remainder of this paper is organized as follows. In Section 2, we detail the system model for the RIS-assisted cooperative NOMA network. In Section 3, we derive the closed-form expressions for the average BLER and effective throughput. Finally, simulation results and concluding remarks are provided in Section 4 and Section 5, respectively.

2. System Model

As shown in Figure 1, we consider a RIS-assisted cooperative NOMA network utilizing short-packet transmission with hardware impairments. The system comprises a single-antenna BS, two single-antenna users, i.e., a near user U_1 and a far user U_2, and a RIS with M reflecting elements. Similar to [27,37], we assume that obstacles block the direct links between the BS and both users ($U_i, i \in 1, 2$), thus necessitating the use of

the RIS for reliable transmission. This assumption is based on the negligible impact of the direct links when the number of RIS elements is large [38]. To evaluate the theoretical performance gain and derive meaningful insights regarding the interplay between RIS and cooperative NOMA, we assume that the BS possesses perfect channel state information (CSI) for all communication links. Although achieving perfect CSI is generally challenging, numerous studies have recently introduced effective channel estimation techniques suitable for RIS-assisted wireless networks, which can be incorporated into our system to obtain accurate CSI [39,40]. For example, Wei et al. [39] proposed an alternating least squares method to achieve continuous and low-complexity estimation of all channels. Moreover, compressive sensing and deep learning were used by Taha et al. [40] to develop two new channel estimation schemes for RIS-assisted wireless systems. The data transmission procedure consists of two phases. In the first phase, BS broadcasts a superimposed signal x containing b_1 bits for U_1 and b_2 bits for U_2 with power P over blocklength L. Subsequently, U_1 serves as a DF relay, processing, and retransmitting signals intended for U_2 in the second phase.

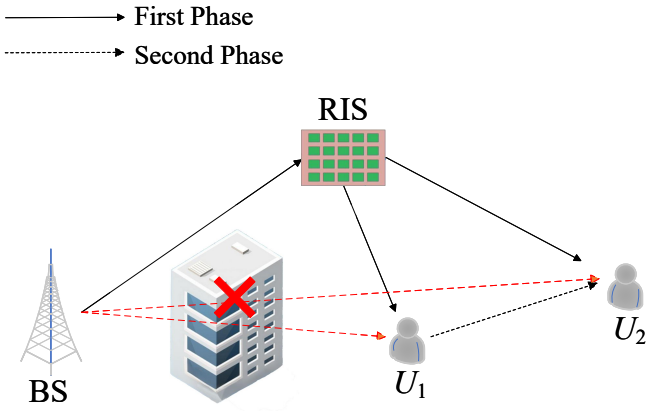


Figure 1. System Model.

According to NOMA scheme [31], the signal x can be expressed as

$$x = \sqrt{\alpha_1 P} x_1 + \sqrt{\alpha_2 P} x_2, \tag{1}$$

where x_1 and x_2 are the signals intended for U_1 and U_2, and α_1 and α_2 are the power allocation factors for U_1 and U_2, respectively. Furthermore, the power allocation factors are constrained by $\alpha_1 + \alpha_2 = 1$ and $\alpha_1 < \alpha_2$. Thus, the signals received at U_1 and U_2 are given by

$$y_{U_1} = \mathbf{h}_{BI}^H \Theta \mathbf{h}_{IU_1} (x + \tau_{BS}^t) + \tau_{U_1}^r + n_{U_1}, \tag{2}$$

and

$$y_{U_2}^1 = \mathbf{h}_{BI}^H \Theta \mathbf{h}_{IU_2} (x + \tau_{BS}^t) + \tau_{U_2}^{r_1} + n_{U_2}^1, \tag{3}$$

where $\mathbf{h}_{BI} = [h_{BI,1}, \cdots, h_{BI,l}, \cdots h_{BI,M}]^H$ is the $M \times 1$ channel vector for the $BS \rightarrow RIS$ link, and $h_{BI,l}$ is the channel coefficient from the BS to the l-th reflecting element of the RIS, $\mathbf{h}_{IU_1} = [h_{IU_1,1}, \cdots, h_{IU_1,l}, \cdots h_{IU_1,M}]^H$ is the $M \times 1$ channel vector for the $RIS \rightarrow U_1$ link, and $h_{IU_1,l}$ is the channel coefficient from the l-th reflecting element of the RIS to U_1, $\mathbf{h}_{IU_2} = [h_{IU_2,1}, \cdots, h_{IU_2,l}, \cdots h_{IU_2,M}]^H$ is the $M \times 1$ channel vector for the $RIS \rightarrow U_2$ link, and $h_{IU_2,l}$ is the channel coefficient from the l-th reflecting element of the RIS to U_2. The diagonal phase shifting matrix of the RIS is denoted by

$\Theta = diag\{e^{j\phi_1}, e^{j\phi_2}, \cdots, e^{j\phi_l}, \cdots, e^{j\phi_M}\}$, where $\phi_l \in [0, 2\pi)$ is the phase shift applied at the l-th reflecting element of the RIS. In addition, $\tau_{BS}^t \sim \mathcal{CN}(0, k_1^2 P)$ is the transmission distortion at the BS, $\tau_{U_1}^r \sim \mathcal{CN}\left(0, k_2^2 P \left|\mathbf{h}_{BI}^H \Theta \mathbf{h}_{IU_1}\right|^2\right)$ is the reception distortion at U_1 and $\tau_{U_2}^{r_1} \sim \mathcal{CN}\left(0, k_2^2 P \left|\mathbf{h}_{BI}^H \Theta \mathbf{h}_{IU_2}\right|^2\right)$ is the reception distortion at U_2. $n_{U_1} \sim \mathcal{CN}(0, \sigma^2)$ and $n_{U_2}^1 \sim \mathcal{CN}(0, \sigma^2)$ are the additive white Gaussian noise (AWGN) at U_1 and U_2, respectively. All channels undergo Nakagami-m fading, i.e., $\left|\mathrm{h}_{BI,l}\right| \sim Nakagami(m_{BI}, \Omega_{BI})$, $\left|\mathrm{h}_{IU_1,l}\right| \sim Nakagami(m_{IU_1}, \Omega_{IU_1})$, $\left|\mathrm{h}_{IU_2,l}\right| \sim Nakagami(m_{IU_2}, \Omega_{IU_2})$. Here, m_{BI} , m_{IU_1} , and m_{IU_2} denote the corresponding distribution parameters, and Ω_{BI} , Ω_{IU_1} , and Ω_{IU_2} represent the corresponding fading means.

According to (2), the instantaneous signal-to-interference-plus-noise ratio (SINR) received to decode x_2 at U_1 in the first phase is given by

$$\gamma_{1,2} = \frac{\alpha_2 \rho \left|\mathbf{h}_{BI}^H \Theta \mathbf{h}_{IU_1}\right|^2}{(\alpha_1 + k_1^2 + k_2^2)\rho \left|\mathbf{h}_{BI}^H \Theta \mathbf{h}_{IU_1}\right|^2 + 1}, \tag{4}$$

where $\rho = \frac{P}{\sigma^2}$ is the transmit signal-to-noise ratio (SNR). Following the finite blocklength analysis in [24], the instantaneous BLER for decoding x_2 at U_1 can be formulated as

$$\varepsilon_{1,2} \approx \Psi(\gamma_{1,2}, b_2, L), \tag{5}$$

where $\Psi(\gamma_{1,2}, b_2, L) \triangleq Q\left(\ln 2 \frac{\log_2(1+\gamma_{1,2}) - b_2/L}{\sqrt{V(\gamma_{1,2})/L}}\right)$, $V(x) = 1 - (1+x)^{-2}$ and $Q(x) = \frac{1}{2\pi}\int_x^\infty e^{-\frac{t^2}{2}} dt$. After successfully decoding and removing x_2 via SIC, U_1 then decodes its own signal x_1. Thus, the instantaneous SINR received to decode x_1 at U_1 in the first phase can be expressed as

$$\gamma_{1,1} = \frac{\alpha_1 \rho \left|\mathbf{h}_{BI}^H \Theta \mathbf{h}_{IU_1}\right|^2}{(k_1^2 + k_2^2)\rho \left|\mathbf{h}_{BI}^H \Theta \mathbf{h}_{IU_1}\right|^2 + 1}. \tag{6}$$

Then, the instantaneous BLER at U_1 is expressed as

$$\varepsilon_{U_1} = \varepsilon_{1,2} + (1 - \varepsilon_{1,2})\varepsilon_{1,1}, \tag{7}$$

where $\varepsilon_{1,1} \approx \Psi(\gamma_{1,1}, b_1, L)$.

According to (3), the instantaneous SINR received to decode x_2 at U_2 in the first phase can be given by

$$\gamma_{2,2}^1 = \frac{\alpha_2 \rho \left|\mathbf{h}_{BI}^H \Theta \mathbf{h}_{IU_2}\right|^2}{(\alpha_1 + k_1^2 + k_2^2)\left|\mathbf{h}_{BI}^H \Theta \mathbf{h}_{IU_2}\right|^2 + 1}. \tag{8}$$

During the second phase, the signal x_2 is cooperatively sent by U_1 to U_2 with the transmit power φP, where $0 < \varphi \leqslant 1$. Thus, the received signal at U_2 is given by

$$y_{U_2}^2 = \sqrt{\varphi P} h_{U_1U_2}(x_2 + \tau_{U_1}^t) + \tau_{U_2}^{r_2} + n_{U_2}^2, \tag{9}$$

where $\left|\mathrm{h}_{U_1U_2}\right| \sim Nakagami(m_{U_1U_2}, \Omega_{U_1U_2})$ is the Nakagami-m fading channel coefficient from U_1 to U_2. Here, $m_{U_1U_2}$ is the distribution parameter, and $\Omega_{U_1U_2}$ is the fading mean. Besides, $\tau_{U_1}^t \sim \mathcal{CN}(0, k_1^2)$ is the transmission distortion at U_1, $\tau_{U_2}^{r_2} \sim \mathcal{CN}\left(0, k_2^2 \varphi P \left|h_{U_1U_2}\right|^2\right)$

is the reception distortion at U_2, and $n_{U_2}^2 \sim \mathcal{CN}(0, \sigma^2)$ is the AWGN at U_2. Therefore, the instantaneous SINR received to decode x_2 at U_2 in the second phase is given by

$$\gamma_{2,2}^2 = \frac{\varphi\rho\left|h_{U_1U_2}\right|^2}{\left(k_1^2 + k_2^2\right)\varphi\rho\left|h_{U_1U_2}\right|^2 + 1}. \tag{10}$$

To improve signal detection at U_2, we consider both SC and MRC schemes to combine the received signals during the first and second phases. For the SC scheme, the instantaneous SINR received to decode x_2 at U_2 is given by

$$\gamma_{2,2}^{SC} = \max\left(\gamma_{2,2}^1, \gamma_{2,2}^2\right). \tag{11}$$

For the MRC scheme, we have

$$\gamma_{2,2}^{MRC} = \gamma_{2,2}^1 + \gamma_{2,2}^2. \tag{12}$$

Thus, the instantaneous BLER for decoding x_2 at U_2 using the SC scheme is expressed as

$$\varepsilon_{U_2^{SC}} = \varepsilon_{1,2}\Psi\left(\gamma_{2,2}^1, b_2, L\right) + (1 - \varepsilon_{1,2})\Psi\left(\gamma_{2,2}^{SC}, b_2, L\right), \tag{13}$$

and the instantaneous BLER for decoding x_2 at U_2 using the MRC scheme is expressed as

$$\varepsilon_{U_2^{MRC}} = \varepsilon_{1,2}\Psi\left(\gamma_{2,2}^1, b_2, L\right) + (1 - \varepsilon_{1,2})\Psi\left(\gamma_{2,2}^{MRC}, b_2, L\right). \tag{14}$$

3. Performance Analysis

In this section, we consider the NUPS and FUPS. For the NUPS, the RIS phase shifts are configured to enhance the channel conditions for the near user, i.e., $\phi_l^1 = -\arg\left(h_{IU_1,l}\right) - \arg(h_{BI,l})$. For the FUPS, the RIS phase shifts are configured to enhance the channel conditions for the far user, i.e., $\phi_l^2 = -\arg\left(h_{IU_2,l}\right) - \arg(h_{BI,l})$. Then, we conduct a comprehensive performance analysis for the near and far users. To characterize the fundamental performance limits of RIS, we assume that the phase shifts can be adjusted continuously within $[0, 2\pi)$, whereas in practical applications they are typically chosen from a discrete set of values ranging from 0 to 2π for simpler hardware implementation. The configuration of RIS utilizing discrete phase shifts will be addressed in future research.

3.1. Preliminaries

According to (4), the cumulative distribution function (CDF) of $\gamma_{1,2}$ under the NUPS can be expressed as

$$\begin{aligned} F_{\gamma_{1,2}^{NUPS}}(x) = &\left(H(x) - H\left(x - \frac{\alpha_2}{\alpha_1 + k_1^2 + k_2^2}\right)\right) \\ &\times \frac{\gamma\left(k_{G_1}, \theta_{G_1}\sqrt{\frac{x}{\alpha_2\rho - \left(\alpha_1 + k_1^2 + k_2^2\right)\rho x}}\right)}{\Gamma\left(k_{G_1}\right)} \\ &+ H\left(x - \frac{\alpha_2}{\alpha_1 + k_1^2 + k_2^2}\right), \end{aligned} \tag{15}$$

where $k_{G_1} = \frac{M\nu_1^2}{\Omega_{BI}\Omega_{IU_1} - \nu_1^2}$, $\theta_{G_1} = \frac{\nu_1}{\Omega_{BI}\Omega_{IU_1} - \nu_1^2}$, $\nu_1 = \frac{\Gamma\left(m_{BI} + \frac{1}{2}\right)\Gamma\left(m_{IU_1} + \frac{1}{2}\right)\sqrt{\Omega_{BI}\Omega_{IU_1}}}{\Gamma(m_{BI})\Gamma\left(m_{IU_1}\right)\sqrt{m_{BI}m_{IU_1}}}$, $\gamma(\alpha, x) = \int_0^x e^{-t}t^{\alpha-1}dt$, $\Gamma(x) = \int_0^\infty e^{-t}t^{x-1}dt$, and $H(x) = \begin{cases} 1, & x > 0 \\ 0, & x \leq 0 \end{cases}$.

Proof. See Appendix A.

Using a method similar to that described in Appendix A, the CDF of $\gamma_{1,1}$ under the NUPS can be expressed as

$$\begin{aligned} F_{\gamma_{1,1}^{NUPS}}(x) = &\left(H(x) - H\left(x - \frac{\alpha_1}{k_1^2 + k_2^2}\right)\right) \\ &\times \frac{\gamma\left(k_{G_1}, \theta_{G_1}\sqrt{\frac{x}{\alpha_1\rho - \left(k_1^2+k_2^2\right)\rho x}}\right)}{\Gamma\left(k_{G_1}\right)} \\ &+ H\left(x - \frac{\alpha_1}{k_1^2 + k_2^2}\right). \end{aligned} \tag{16}$$

According to [41], $\left|\mathbf{h}_{BI}^H \Theta \mathbf{h}_{IU_2}\right|^2$ can be approximated by a Rayleigh distribution, i.e., $\left|\mathbf{h}_{BI}^H \Theta \mathbf{h}_{IU_2}\right|^2 \sim \mathcal{CN}\left(0, M\Omega_{BI}\Omega_{IU_2}\right)$. Then, through straightforward mathematical derivations, the CDF of $\gamma_{2,2}^1$ under the NUPS can be formulated as

$$\begin{aligned} F_{\gamma_{2,2}^{1,NUPS}}(x) = &\left(H(x) - H\left(x - \frac{\alpha_2}{\alpha_1 + k_1^2 + k_2^2}\right)\right) \\ &\times \left(1 - e^{-\frac{x}{M\Omega_{BI}\Omega_{IU_2}\left(\alpha_2\rho - \left(\alpha_1 + k_1^2 + k_2^2\right)\rho x\right)}}\right) \\ &+ H\left(x - \frac{\alpha_2}{\alpha_1 + k_1^2 + k_2^2}\right). \end{aligned} \tag{17}$$

Due to the independence between the relay and reflection links, the CDF of $\gamma_{2,2}^2$ is identical for both the FUPS and NUPS. Since the CDF of $\left|h_{U_1U_2}\right|^2$ can be expressed as $F_{\left|h_{U_1U_2}\right|^2}(x) = \frac{\gamma\left(m_{U_1U_2}, \frac{m_{U_1U_2}x}{\Omega_{U_1U_2}}\right)}{\Gamma\left(m_{U_1U_2}\right)}$, thus, the CDF of $\gamma_{2,2}^2$ can be expressed as

$$\begin{aligned} F_{\gamma_{2,2}^2}(x) = &\left(H(x) - H\left(x - \frac{1}{k_1^2 + k_2^2}\right)\right) \\ &\times \frac{\gamma\left(m_{U_1U_2}, \frac{m_{U_1U_2}x}{\Omega_{U_1U_2}\left(\varphi\rho - \left(k_1^2+k_2^2\right)\varphi\rho x\right)}\right)}{\Gamma\left(m_{U_1U_2}\right)} \\ &+ H\left(x - \frac{1}{k_1^2 + k_2^2}\right). \end{aligned} \tag{18}$$

Under the FUPS, $\left|\mathbf{h}_{BI}^H \Theta \mathbf{h}_{IU_1}\right|^2$ can be approximated as an exponential distribution with mean $M\Omega_{BI}\Omega_{IU_1}$. Thus, the CDFs of $\gamma_{1,2}$ and $\gamma_{1,1}$ under the FUPS can be, respectively, expressed as

$$\begin{aligned} F_{\gamma_{1,2}^{FUPS}}(x) = &\left(H(x) - H\left(x - \frac{\alpha_2}{\alpha_1 + k_1^2 + k_2^2}\right)\right) \\ &\times \left(1 - e^{-\frac{x}{M\Omega_{BI}\Omega_{IU_1}\left(\alpha_2\rho - \left(\alpha_1 + k_1^2 + k_2^2\right)\rho x\right)}}\right) \\ &+ H\left(x - \frac{\alpha_2}{\alpha_1 + k_1^2 + k_2^2}\right), \end{aligned} \tag{19}$$

and

$$F_{\gamma_{1,1}^{FUPS}}(x) = \left(H(x) - H\left(x - \frac{\alpha_1}{k_1^2 + k_2^2}\right)\right) \times \left(1 - e^{-\frac{x}{M\Omega_{BI}\Omega_{IU_1}\left(\alpha_1\rho - \left(k_1^2+k_2^2\right)\rho x\right)}}\right) + H\left(x - \frac{\alpha_1}{k_1^2 + k_2^2}\right). \tag{20}$$

Based on (8) and following a derivation similar to Appendix A, the CDF of $\gamma_{2,2}^1$ under the FUPS is given by

$$F_{\gamma_{2,2}^{1,FUPS}}(x) = \left(H(x) - H\left(x - \frac{\alpha_2}{\alpha_1 + k_1^2 + k_2^2}\right)\right) \times \frac{\gamma\left(k_{G_2}, \theta_{G_2}\sqrt{\frac{x}{\alpha_2\rho - \left(\alpha_1 + k_1^2 + k_2^2\right)\rho x}}\right)}{\Gamma\left(k_{G_2}\right)} + H\left(x - \frac{\alpha_2}{\alpha_1 + k_1^2 + k_2^2}\right), \tag{21}$$

where $k_{G_2} = \frac{M\nu_2^2}{\Omega_{BI}\Omega_{IU_2} - \nu_2^2}$, $\theta_{G_2} = \frac{\nu_2}{\Omega_{BI}\Omega_{IU_2} - \nu_2^2}$, $\nu_2 = \frac{\Gamma\left(m_{BI}+\frac{1}{2}\right)\Gamma\left(m_{IU_2}+\frac{1}{2}\right)\sqrt{\Omega_{BI}\Omega_{IU_2}}}{\Gamma(m_{BI})\Gamma\left(m_{IU_2}\right)\sqrt{m_{BI}m_{IU_2}}}$. □

3.2. Near-User Priority Strategy

The closed-form expression of the average BLER at U_1 under the NUPS is given by

$$\bar{\varepsilon}_{U_1}^{NUPS} \approx \mathbb{E}\left(\varepsilon_{1,2}^{NUPS}\right) + \mathbb{E}\left(\varepsilon_{1,1}^{NUPS}\right), \tag{22}$$

where $\mathbb{E}(\cdot)$ denotes the expectation operator, $\mathbb{E}\left(\varepsilon_{1,2}^{NUPS}\right)$ and $\mathbb{E}\left(\varepsilon_{1,1}^{NUPS}\right)$ are given by

$$\begin{aligned}\mathbb{E}\left(\varepsilon_{1,2}^{NUPS}\right) &= H(A_2) - H\left(\frac{\alpha_2}{\alpha_1 + k_1^2 + k_2^2} - A_2\right) + \left(H(B_2) - H\left(B_2 - \frac{\alpha_2}{\alpha_1 + k_1^2 + k_2^2}\right)\right) \\ &\times \sum_{n=1}^{N} \frac{\pi g_2\sqrt{L}(B_2 - A_2)}{2N\Gamma\left(k_{G_1}\right)}\sqrt{1 - t_n^2}\,\gamma\left(k_{G_1}, \theta_{G_1}\sqrt{\frac{\mu_1}{\alpha_2\rho - \left(\alpha_1 + k_1^2 + k_2^2\right)\rho\mu_1}}\right) \\ &+ \left(H\left(\frac{\alpha_2}{\alpha_1 + k_1^2 + k_2^2} - A_2\right) - H\left(\frac{\alpha_2}{\alpha_1 + k_1^2 + k_2^2} - B_2\right)\right) \times \left(\frac{1}{2} - g_2\sqrt{L}\right. \\ &\times \left(\frac{\alpha_2}{\alpha_1 + k_1^2 + k_2^2} - h_2\right) + \sum_{n=1}^{N} \frac{\pi g_2\sqrt{L}\left(\alpha_2 - A_2\left(\alpha_1 + k_1^2 + k_2^2\right)\right)}{2N\left(\alpha_1 + k_1^2 + k_2^2\right)\Gamma\left(k_{G_1}\right)}\sqrt{1 - t_n^2} \\ &\left.\times\gamma\left(k_{G_1}, \theta_{G_1}\sqrt{\frac{\mu_2}{\alpha_2\rho - \left(\alpha_1 + k_1^2 + k_2^2\right)\rho\mu_2}}\right)\right),\end{aligned} \tag{23}$$

and

$$\mathbb{E}\left(\varepsilon_{1,1}^{NUPS}\right) = H(A_1) - H\left(\frac{\alpha_1}{k_1^2+k_2^2} - A_1\right) + \left(H(B_1) - H\left(B_1 - \frac{\alpha_1}{k_1^2+k_2^2}\right)\right) \times \sum_{n=1}^{N} \frac{\pi g_1 \sqrt{L}(B_1 - A_1)}{2N\Gamma\left(k_{G_1}\right)} \sqrt{1-t_n^2}\gamma\left(k_{G_1}, \theta_{G_1}\sqrt{\frac{\mu_3}{\alpha_1\rho - (k_1^2+k_2^2)\rho\mu_3}}\right) + \left(H\left(\frac{\alpha_1}{k_1^2+k_2^2} - A_1\right) - H\left(\frac{\alpha_1}{k_1^2+k_2^2} - B_1\right)\right) \times \left(\frac{1}{2} - g_1\sqrt{L} \times \left(\frac{\alpha_1}{k_1^2+k_2^2} - h_1\right) + \sum_{n=1}^{N} \frac{\pi g_1 \sqrt{L}(\alpha_1 - A_1(k_1^2+k_2^2))}{2N(k_1^2+k_2^2)\Gamma\left(k_{G_1}\right)} \sqrt{1-t_n^2} \times\gamma\left(k_{G_1}, \theta_{G_1}\sqrt{\frac{\mu_4}{\alpha_1\rho - (k_1^2+k_2^2)\rho\mu_4}}\right)\right), \tag{24}$$

with $h_2 = 2^{\frac{b_2}{L}} - 1$, $g_2 = \left(2\pi\left(2^{\frac{2b_2}{L}} - 1\right)\right)^{-\frac{1}{2}}$, $A_2 = h_2 - \frac{1}{2g_2\sqrt{L}}$, $B_2 = h_2 + \frac{1}{2g_2\sqrt{L}}$, $\mu_1 = \frac{B_2 - A_2}{2} t_n + \frac{B_2 + A_2}{2}$, $t_n = \cos\left(\frac{2n-1}{2N}\pi\right)$, $\mu_2 = \frac{\alpha_2 - A_2\left(\alpha_1 + k_1^2 + k_2^2\right)}{2\left(\alpha_1 + k_1^2 + k_2^2\right)} t_n + \frac{\alpha_2 + A_2\left(\alpha_1 + k_1^2 + k_2^2\right)}{2\left(\alpha_1 + k_1^2 + k_2^2\right)}$, $h_1 = 2^{\frac{b_1}{L}} - 1$, $g_1 = \left(2\pi\left(2^{\frac{2b_1}{L}} - 1\right)\right)^{-\frac{1}{2}}$, $A_1 = h_1 - \frac{1}{2g_1\sqrt{L}}$, $B_1 = h_1 + \frac{1}{2g_1\sqrt{L}}$, $\mu_3 = \frac{B_1 - A_1}{2} t_n + \frac{B_1 + A_1}{2}$, $\mu_4 = \frac{\alpha_1 - A_1\left(k_1^2 + k_2^2\right)}{2\left(k_1^2 + k_2^2\right)} t_n + \frac{\alpha_1 + A_1\left(k_1^2 + k_2^2\right)}{2\left(k_1^2 + k_2^2\right)}$, and N being a parameter for the complexity accuracy tradeoff.

Proof. See Appendix B.

For the SC scheme, the closed-form expression of the average BLER at U_2 under the NUPS is given by

$$\bar{\varepsilon}_{U_2^{SC}}^{NUPS} = \mathbb{E}\left(\varepsilon_{1,2}^{NUPS}\right)\mathbb{E}\left(\Psi\left(\gamma_{2,2}^{1,NUPS}, b_2, L\right)\right) + \left(1 - \mathbb{E}\left(\varepsilon_{1,2}^{NUPS}\right)\right)\mathbb{E}\left(\Psi\left(\gamma_{2,2}^{SC,NUPS}, b_2, L\right)\right), \tag{25}$$

where $\mathbb{E}\left(\Psi\left(\gamma_{2,2}^{1,NUPS}, b_2, L\right)\right)$ is expressed as

$$\mathbb{E}\left(\Psi\left(\gamma_{2,2}^{1,NUPS}, b_2, L\right)\right) = \left(1 - \frac{g_2\sqrt{L}\alpha_2 e^{\frac{1}{p_1}}}{p_1^2\left(\rho M \Omega_{BI}\Omega_{IU_2}\right)^{-1}}\left(\zeta\left(A_2^1 + p_1\right) - \zeta\left(B_2^1 + p_1\right)\right)\right) \times \left(H(B_2) - H\left(B_2 - \frac{\alpha_2}{\alpha_1 + k_1^2 + k_2^2}\right)\right) + \left(H\left(\frac{\alpha_2}{\alpha_1 + k_1^2 + k_2^2} - A_2\right) - H\left(\frac{\alpha_2}{\alpha_1 + k_1^2 + k_2^2} - B_2\right)\right)\left(\frac{1}{2} - \frac{g_2\sqrt{L}\alpha_2 e^{\frac{1}{p_1}}}{p_1^2\left(\rho M \Omega_{BI}\Omega_{IU_2}\right)^{-1}}\left(\zeta\left(A_2^1 + p_1\right) - \zeta\left(\frac{1}{2p_1} + p_1\right)\right)\right) + H(A_2) - H\left(\frac{\alpha_2}{\alpha_1 + k_1^2 + k_2^2} - A_2\right), \tag{26}$$

with $p_1 = \rho M \Omega_{BI}\Omega_{IU_2}\left(\alpha_1 + k_1^2 + k_2^2\right)$, $A_2^1 = \frac{A_2}{\left(\alpha_2\rho + \left(\alpha_1 + k_1^2 + k_2^2\right)\rho A_2\right)M\Omega_{BI}\Omega_{IU_2}}$, $B_2^1 = \frac{B_2}{\left(\alpha_2\rho + \left(\alpha_1 + k_1^2 + k_2^2\right)\rho B_2\right)M\Omega_{BI}\Omega_{IU_2}}$ and $\zeta(x) = \mathrm{Ei}(-x) + \frac{e^{-x}}{x}$. □

Proof. See Appendix C.

Note that directly computing $\mathbb{E}\left(\Psi\left(\gamma_{2,2}^{SC,NUPS}, b_2, L\right)\right)$ is intractable. Inspired by [42], we can use $\mathbb{E}\left(\Psi\left(\gamma_{2,2}^{1,NUPS}, b_2, L\right)\right)\mathbb{E}\left(\Psi\left(\gamma_{2,2}^{2}, b_2, L\right)\right)$ as an approximation for $\mathbb{E}\left(\Psi\left(\gamma_{2,2}^{SC,NUPS}, b_2, L\right)\right)$. Based on (18), following a similar procedure to Appendix B, $\mathbb{E}\left(\Psi\left(\gamma_{2,2}^{2}, N_2, L\right)\right)$ can be derived as

$$\begin{aligned}\mathbb{E}\left(\Psi\left(\gamma_{2,2}^{2}, b_2, L\right)\right) = &\sum_{n=1}^{N} \frac{\pi g_2\sqrt{L}(B_2-A_2)}{2N\Gamma\left(m_{U_1U_2}\right)}\sqrt{1-t_n^2}\gamma\left(m_{U_1U_2}, \frac{m_{U_1U_2}}{\Omega_{U_1U_2}}\mu_5\right)\\ &\times\left(H(B_2)-H\left(B_2-\frac{1}{k_1^2+k_2^2}\right)\right)+\left(H\left(\frac{1}{k_1^2+k_2^2}-A_2\right)\right.\\ &\left.-H\left(\frac{1}{k_1^2+k_2^2}-B_2\right)\right)\left(\frac{1}{2}-g_2\sqrt{L}\left(\frac{1}{k_1^2+k_2^2}-h_2\right)+g_2\sqrt{L}\right.\\ &\left.\times\sum_{n=1}^{N}\frac{\pi\left(1-A_2\left(k_1^2+k_2^2\right)\right)}{2N\left(k_1^2+k_2^2\right)\Gamma\left(m_{U_1U_2}\right)}\sqrt{1-t_n^2}\gamma\left(m_{U_1U_2}, \frac{m_{U_1U_2}}{\Omega_{U_1U_2}}\mu_6\right)\right)\\ &+H(A_2)-H\left(\frac{1}{k_1^2+k_2^2}-A_2\right),\end{aligned} \tag{27}$$

with $\mu_5 = \frac{(B_2-A_2)t_n+A_2+B_2}{\varphi\rho\left(2-\left(k_1^2+k_2^2\right)\left((B_2-A_2)t_n+A_2+B_2\right)\right)}$, and $\mu_6 = \frac{\left(1-\left(k_1^2+k_2^2\right)A_2\right)t_n+\left(k_1^2+k_2^2\right)A_2+1}{\left(k_1^2+k_2^2\right)\varphi\rho\left(1-\left(1-\left(k_1^2+k_2^2\right)A_2\right)t_n-\left(k_1^2+k_2^2\right)A_2\right)}$.

For the MRC scheme, the closed-form expression of the average BLER at U_2 under the NUPS is given by

$$\begin{aligned}\bar{\varepsilon}_{U_2^{MRC}}^{NUPS} = &\mathbb{E}\left(\varepsilon_{1,2}^{NUPS}\right)\mathbb{E}\left(\Psi\left(\gamma_{2,2}^{1,NUPS}, b_2, L\right)\right)\\ &+\left(1-\mathbb{E}\left(\varepsilon_{1,2}^{NUPS}\right)\right)\mathbb{E}\left(\Psi\left(\gamma_{2,2}^{MRC,NUPS}, b_2, L\right)\right).\end{aligned} \tag{28}$$

According to the approximation method in [43], $\mathbb{E}\left(\Psi\left(\gamma_{2,2}^{MRC,NUPS}, b_2, L\right)\right)$ can be approximated as $\mathbb{E}\left(\Psi\left(2\gamma_{2,2}^{1,NUPS}, b_2, L\right)\right)\mathbb{E}\left(\Psi\left(2\gamma_{2,2}^{2}, b_2, L\right)\right)$. Following a similar procedure to Appendix C, we can express $\mathbb{E}\left(\Psi\left(2\gamma_{2,2}^{1,NUPS}, b_2, L\right)\right)$ and $\mathbb{E}\left(\Psi\left(2\gamma_{2,2}^{2}, b_2, L\right)\right)$ as

$$\begin{aligned}\mathbb{E}\left(\Psi\left(2\gamma_{2,2}^{1,NUPS}, b_2, L\right)\right) = &\left(1-\frac{2g_2\sqrt{L}\alpha_2 e^{\frac{1}{p_1}}}{p_1^2\left(\rho M\Omega_{BI}\Omega_{IU_2}\right)^{-1}}\left(\zeta\left(\frac{A_2^1}{2}+p_1\right)-\zeta\left(\frac{B_2^1}{2}+p_1\right)\right)\right)\\ &\times\left(H\left(\frac{B_2}{2}\right)-H\left(\frac{B_2}{2}-\frac{\alpha_2}{\alpha_1+k_1^2+k_2^2}\right)\right)+\left(\frac{1}{2}-2g_2\sqrt{L}\right.\\ &\left.\times\frac{\alpha_2 e^{\frac{1}{p_1}}}{p_1^2\left(\rho M\Omega_{BI}\Omega_{IU_2}\right)^{-1}}\left(\zeta\left(\frac{A_2^1}{2}+p_1\right)-\zeta\left(\frac{1}{4p_1}+p_1\right)\right)\right)\\ &\times\left(H\left(\frac{\alpha_2}{\alpha_1+k_1^2+k_2^2}-\frac{A_2}{2}\right)-H\left(\frac{\alpha_2}{\alpha_1+k_1^2+k_2^2}-\frac{B_2}{2}\right)\right)\\ &+H\left(\frac{A_2}{2}\right)-H\left(\frac{\alpha_2}{\alpha_1+k_1^2+k_2^2}-\frac{A_2}{2}\right),\end{aligned} \tag{29}$$

and

$$\begin{aligned}\mathbb{E}\left(\Psi\left(2\gamma_{2,2}^2, b_2, L\right)\right) &= H\left(\frac{A_2}{2}\right) - H\left(\frac{1}{k_1^2+k_2^2} - \frac{A_2}{2}\right) + \left(\frac{1}{2} - g_2\sqrt{L}\left(\frac{2}{k_1^2+k_2^2} - h_2\right)\right.\\ &\left. + \sum_{n=1}^{N} \frac{\pi g_2\sqrt{L}\left(2 - A_2\left(k_1^2+k_2^2\right)\right)}{2N\left(k_1^2+k_2^2\right)\Gamma\left(m_{U_1U_2}\right)}\sqrt{1-t_n^2}\gamma\left(m_{U_1U_2}, \frac{m_{U_1U_2}}{\Omega_{U_1U_2}}\mu_7\right)\right)\\ &\times \left(H\left(\frac{1}{k_1^2+k_2^2} - \frac{A_2}{2}\right) - H\left(\frac{1}{k_1^2+k_2^2} - \frac{B_2}{2}\right)\right) + g_2\sqrt{L}\\ &\times \sum_{n=1}^{N} \frac{\pi(B_2 - A_2)}{2N\Gamma\left(m_{U_1U_2}\right)}\sqrt{1-t_n^2}\gamma\left(m_{U_1U_2}, \frac{m_{U_1U_2}}{\Omega_{U_1U_2}}\mu_8\right)\\ &\times \left(H\left(\frac{B_2}{2}\right) - H\left(\frac{B_2}{2} - \frac{1}{k_1^2+k_2^2}\right)\right),\end{aligned} \tag{30}$$

with $\mu_7 = \frac{\left(2-\left(k_1^2+k_2^2\right)A_2\right)t_n+\left(k_1^2+k_2^2\right)A_2+2}{\left(k_1^2+k_2^2\right)\varphi\rho\left(2-\left(2-\left(k_1^2+k_2^2\right)A_2\right)t_n-\left(k_1^2+k_2^2\right)A_2\right)}$, and $\mu_8 = \frac{(B_2-A_2)t_n+A_2+B_2}{\varphi\rho\left(4-\left(k_1^2+k_2^2\right)((B_2-A_2)t_n+A_2+B_2)\right)}$. □

3.3. Far-User Priority Strategy

The closed-form expression of the average BLER at U_1 under the FUPS is given by

$$\bar{\varepsilon}_{U_1}^{FUPS} \approx \mathbb{E}\left(\varepsilon_{1,2}^{FUPS}\right) + \mathbb{E}\left(\varepsilon_{1,1}^{FUPS}\right), \tag{31}$$

Similar to Appendix C, $\mathbb{E}\left(\varepsilon_{1,2}^{FUPS}\right)$ and $\mathbb{E}\left(\varepsilon_{1,1}^{FUPS}\right)$ are given by

$$\begin{aligned}\mathbb{E}\left(\varepsilon_{1,2}^{FUPS}\right) &= H(A_2) - H\left(\frac{\alpha_2}{\alpha_1+k_1^2+k_2^2} - A_2\right) + \left(H(B_2) - H\left(B_2 - \frac{\alpha_2}{\alpha_1+k_1^2+k_2^2}\right)\right)\\ &\times \left(1 - \frac{g_2\sqrt{L}\alpha_2 e^{\frac{1}{p_2}}}{p_2^2\left(\rho M\Omega_{BI}\Omega_{IU_1}\right)^{-1}}\left(\zeta\left(A_2^2+p_2\right) - \zeta\left(B_2^2+p_2\right)\right)\right)\\ &+ \left(\frac{1}{2} - \frac{g_2\sqrt{L}\alpha_2 e^{\frac{1}{p_2}}}{p_2^2\left(\rho M\Omega_{BI}\Omega_{IU_1}\right)^{-1}}\left(\zeta\left(A_2^2+p_2\right) - \zeta\left(\frac{1}{2p_2}+p_2\right)\right)\right)\\ &\times \left(H\left(\frac{\alpha_2}{\alpha_1+k_1^2+k_2^2} - A_2\right) - H\left(\frac{\alpha_2}{\alpha_1+k_1^2+k_2^2} - B_2\right)\right),\end{aligned} \tag{32}$$

and

$$\begin{aligned}\mathbb{E}\left(\varepsilon_{1,1}^{FUPS}\right) &= H(A_1) - H\left(\frac{\alpha_1}{k_1^2+k_2^2} - A_1\right) + \left(H\left(\frac{\alpha_1}{k_1^2+k_2^2} - A_1\right) - H\left(\frac{\alpha_1}{k_1^2+k_2^2} - B_1\right)\right)\\ &\times \left(\frac{1}{2} - \frac{g_1\sqrt{L}\alpha_1 e^{\frac{1}{p_3}}}{p_3^2\left(\rho M\Omega_{BI}\Omega_{IU_1}\right)^{-1}}\left(\zeta\left(A_1^2+p_3\right) - \zeta\left(\frac{1}{2p_3}+p_3\right)\right)\right)\\ &+ \left(1 - \frac{g_1\sqrt{L}\alpha_1 e^{\frac{1}{p_3}}}{p_3^2\left(\rho M\Omega_{BI}\Omega_{IU_1}\right)^{-1}}\left(\zeta\left(A_1^2+p_3\right) - \zeta\left(B_1^2+p_3\right)\right)\right)\\ &\times \left(H(B_1) - H\left(B_1 - \frac{\alpha_1}{k_1^2+k_2^2}\right)\right),\end{aligned} \tag{33}$$

with $A_2^2 = \frac{A_2}{\left(\alpha_2\rho+\left(\alpha_1+k_1^2+k_2^2\right)\rho A_2\right)M\Omega_{BI}\Omega_{IU_1}}$, $B_2^2 = \frac{B_2}{\left(\alpha_2\rho+\left(\alpha_1+k_1^2+k_2^2\right)\rho B_2\right)M\Omega_{BI}\Omega_{IU_1}}$, $A_1^2 = \frac{A_1}{\left(\alpha_1\rho+\left(k_1^2+k_2^2\right)\rho A_1\right)M\Omega_{BI}\Omega_{IU_1}}$, $B_1^2 = \frac{B_1}{\left(\alpha_1\rho+\left(k_1^2+k_2^2\right)\rho B_1\right)M\Omega_{BI}\Omega_{IU_1}}$, $p_2 = \rho M\Omega_{BI}\Omega_{IU_1}\left(\alpha_1+k_1^2+k_2^2\right)$, and $p_3 = \rho M\Omega_{BI}\Omega_{IU_1}\left(k_1^2+k_2^2\right)$.

For the SC scheme, the closed-form expression of the average BLER at U_2 under the FUPS is given by

$$\begin{aligned}\bar{\varepsilon}_{U_2^{SC}}^{FUPS} &= \mathbb{E}\left(\varepsilon_{1,2}^{FUPS}\right)\mathbb{E}\left(\Psi\left(\gamma_{2,2}^{1,FUPS}, b_2, L\right)\right)\\ &\quad+\left(1-\mathbb{E}\left(\varepsilon_{1,2}^{FUPS}\right)\right)\mathbb{E}\left(\Psi\left(\gamma_{2,2}^{SC,FUPS}, b_2, L\right)\right).\end{aligned} \tag{34}$$

Similar to the analysis for the NUPS, $\mathbb{E}\left(\Psi\left(\gamma_{2,2}^{1,FUPS}, b_2, L\right)\right)$ can be expressed as

$$\begin{aligned}\mathbb{E}\left(\Psi\left(\gamma_{2,2}^{1,FUPS}, b_2, L\right)\right) &= H(A_2) - H\left(\frac{\alpha_2}{\alpha_1+k_1^2+k_2^2} - A_2\right) + \left(H\left(\frac{\alpha_2}{\alpha_1+k_1^2+k_2^2} - A_2\right)\right.\\ &\quad\left.-H\left(\frac{\alpha_2}{\alpha_1+k_1^2+k_2^2} - B_2\right)\right) \times \left(\frac{1}{2} - g_2\sqrt{L}\left(\frac{\alpha_2}{\alpha_1+k_1^2+k_2^2} - h_2\right)\right.\\ &\quad+\sum_{n=1}^{N}\frac{\pi g_2\sqrt{L}\left(\alpha_2 - A_2\left(\alpha_1+k_1^2+k_2^2\right)\right)}{2N\left(\alpha_1+k_1^2+k_2^2\right)\Gamma\left(k_{G_2}\right)}\sqrt{1-t_n^2}\\ &\quad\left.\times\gamma\left(k_{G_2}, \theta_{G_2}\sqrt{\frac{\mu_2}{\alpha_2\rho-\left(\alpha_1+k_1^2+k_2^2\right)\rho\mu_2}}\right)\right)\\ &\quad+\left(H(B_2) - H\left(B_2 - \frac{\alpha_2}{\alpha_1+k_1^2+k_2^2}\right)\right)\\ &\quad\times\sum_{n=1}^{N}\frac{\pi g_2\sqrt{L}(B_2-A_2)}{2N\Gamma\left(k_{G_2}\right)}\sqrt{1-t_n^2}\\ &\quad\times\gamma\left(k_{G_2}, \theta_{G_2}\sqrt{\frac{\mu_1}{\alpha_2\rho-\left(\alpha_1+k_1^2+k_2^2\right)\rho\mu_1}}\right),\end{aligned} \tag{35}$$

and $\mathbb{E}\left(\Psi\left(\gamma_{2,2}^{SC,FUPS}, b_2, L\right)\right)$ can be approximated as the product of $\mathbb{E}\left(\Psi\left(\gamma_{2,2}^{1,FUPS}, b_2, L\right)\right)$ and $\mathbb{E}\left(\Psi\left(\gamma_{2,2}^{2}, b_2, L\right)\right)$.

For the MRC scheme, the closed-form expression of the average BLER at U_2 under the FUPS is given by

$$\begin{aligned}\bar{\varepsilon}_{U_2^{MRC}}^{FUPS} &= \mathbb{E}\left(\varepsilon_{1,2}^{FUPS}\right)\mathbb{E}\left(\Psi\left(\gamma_{2,2}^{1,FUPS}, b_2, L\right)\right)\\ &\quad+\left(1-\mathbb{E}\left(\varepsilon_{1,2}^{FUPS}\right)\right)\mathbb{E}\left(\Psi\left(\gamma_{2,2}^{MRC,FUPS}, b_2, L\right)\right).\end{aligned} \tag{36}$$

Employing the same method as applied to the NUPS, $\mathbb{E}\left(\Psi\left(\gamma_{2,2}^{MRC,FUPS}, b_2, L\right)\right)$ can be approximated as the product of $\mathbb{E}\left(\Psi\left(2\gamma_{2,2}^{1,FUPS}, b_2, L\right)\right)$ and $\mathbb{E}\left(\Psi\left(2\gamma_{2,2}^{2}, b_2, L\right)\right)$, where $\mathbb{E}\left(\Psi\left(2\gamma_{2,2}^{1,FUPS}, b_2, L\right)\right)$ is given by

$$\begin{aligned}\mathbb{E}\left(\Psi\left(2\gamma_{2,2}^{1,FUPS}, b_2, L\right)\right) = H\left(\frac{A_2}{2}\right) - H\left(\frac{\alpha_2}{\alpha_1+k_1^2+k_2^2} - \frac{A_2}{2}\right) + \left(H\left(\frac{B_2}{2}\right)\right. \\ \left. -H\left(\frac{B_2}{2} - \frac{\alpha_2}{\alpha_1+k_1^2+k_2^2}\right)\right) \sum_{n=1}^{N} \frac{\pi g_2 \sqrt{L}(B_2-A_2)}{2N\Gamma\left(k_{G_2}\right)} \sqrt{1-t_n^2} \\ \times \gamma\left(k_{G_2}, \theta_{G_2}\sqrt{\frac{\mu_1}{2\alpha_2\rho - (\alpha_1+k_1^2+k_2^2)\rho\mu_1}}\right) + \left(\frac{1}{2} - g_2\sqrt{L}\right. \\ \times \left(\frac{2\alpha_2}{\alpha_1+k_1^2+k_2^2} - h_2\right) + \sum_{n=1}^{N} \frac{\pi g_2\sqrt{L}\left(\alpha_2 - \frac{A_2}{2}\left(\alpha_1+k_1^2+k_2^2\right)\right)}{2N\left(\alpha_1+k_1^2+k_2^2\right)\Gamma\left(k_{G_2}\right)} \\ \times\sqrt{1-t_n^2}\gamma\left(k_{G_2}, \theta_{G_2}\sqrt{\frac{\mu_9}{\alpha_2\rho - (\alpha_1+k_1^2+k_2^2)\rho\mu_9}}\right)\Bigg) \\ \times\left(H\left(\frac{\alpha_2}{\alpha_1+k_1^2+k_2^2} - \frac{A_2}{2}\right) - H\left(\frac{\alpha_2}{\alpha_1+k_1^2+k_2^2} - \frac{B_2}{2}\right)\right),\end{aligned} \tag{37}$$

with $\mu_9 = \frac{2\alpha_2 - A_2\left(\alpha_1+k_1^2+k_2^2\right)}{4\left(\alpha_1+k_1^2+k_2^2\right)} t_n + \frac{2\alpha_2 + A_2\left(\alpha_1+k_1^2+k_2^2\right)}{4\left(\alpha_1+k_1^2+k_2^2\right)}$.

3.4. Effective Throughput

Effective throughput is defined as the average number of information bits successfully decoded per channel use. For the RIS-assisted cooperative NOMA network, the effective throughput is expressed as

$$T^{\star} = \frac{b_1}{L}\left(1 - \bar{\varepsilon}_{U_1}^{\star}\right) + \frac{b_2}{L}\left(1 - \bar{\varepsilon}_{U_2^*}^{\star}\right), \tag{38}$$

where $\star \in \{NUPS, HUPS\}$, $* \in \{SC, MRC\}$, $\frac{b_1}{L}$ and $\frac{b_2}{L}$ represent the information rates of U_1 and U_2, and $\left(1 - \bar{\varepsilon}_{U_1}^{\star}\right)$ and $\left(1 - \bar{\varepsilon}_{U_2^*}^{\star}\right)$ are the reliabilities of U_1 and U_2, respectively. It can be observed that as L increases, the information rate decreases while the user reliability increases. Therefore, there exists an optimal L at which the effective throughput reaches its maximum. However, due to the complexity of the effective throughput expression, an explicit closed-form solution for the optimal blocklength L is difficult to obtain. Nevertheless, a gradient-based search method can be employed to numerically determine the optimal L.

4. Numerical Results

In this section, we present comprehensive simulation results to evaluate the performance of the RIS-assisted cooperative NOMA network. The system's performance is primarily measured in terms of the average BLER and effective throughput, which are derived from the analytical expressions in the previous sections. Unless otherwise specified, the simulation parameters are given in Table 2. The following figures aim to provide key insights into the interplay between RIS configuration, hardware impairments, and the requirements of finite blocklength. The accuracy of our theoretical analysis is validated by the close alignment between the Monte Carlo simulation results and the analytical curve, as evidenced in these figures. The simulations in this work are conducted using a baseband-equivalent model, which is a common methodology for analyzing the fundamental performance of communication systems independent of a specific carrier frequency. This approach allows us to study the core relationship between SNR and BLER, as it is the most direct and critical measure for assessing reliability in short-packet communications. It is important to note that the choice of a carrier frequency in a practical implementation

would directly impact the absolute path loss and fading characteristics. However, in our model, these frequency-dependent propagation effects are implicitly captured by the SNR value at the receiver and the statistical channel model (e.g., Nakagami-m fading) we employ. The presented SNR-BLER curves illustrate the fundamental trade-offs and performance trends. For a specific real-world deployment (e.g., at a sub-6 GHz or millimeter wave frequency bands), the absolute SNR required for a target BLER would be determined by the total link budget, including the frequency-specific path loss, but the relative shape and trends of the curves would remain valid.

Table 2. List of simulation parameters.

Parameter	Value
Blocklength	$L = 200$
Transmit SNR	$\rho = 0$ dB
Number of reflecting elements	$M = 5$
Complexity accuracy tradeoff parameter	$N = 200$
Level of hardware impairments	$k_1 = k_2 = 0.1$
Distribution parameters	$m_{BI} = m_{IU_1} = m_{IU_2} = m_{U_1U_2} = 2$
Fading means	$\Omega_{BI} = \Omega_{IU_2} = 0$ dB, $\Omega_{IU_1} = 5$ dB, $\Omega_{U_1U_2} = 10$ dB
Number of information bits	$b_1 = b_2 = 200$
Power allocation coefficient	$a_1 = 0.1$, $\varphi = 0.5$

Figure 2 plots the average BLER under the NUPS and FUPS versus ρ. For comparison, the average BLER of the far user in the conventional non-cooperative NOMA network is also provided, denoted as U_2^{Non}. As ρ increases, the average BLER decreases for the near and far users, which is attributed to the corresponding rise in received SNR. Moreover, the average BLER of the far user under the NUPS and FUPS is lower than that in the conventional non-cooperative NOMA network. In the NUPS, MRC demonstrates a clear performance advantage over SC.

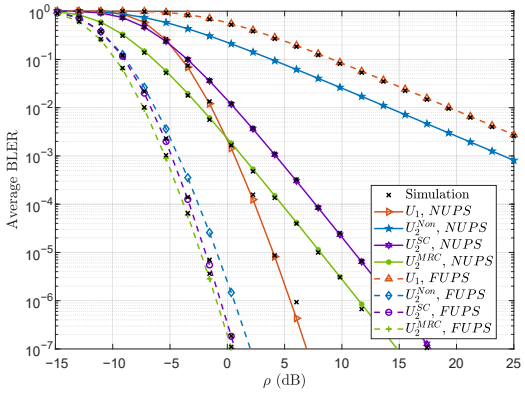


Figure 2. Average BLER under the NUPS and FUPS versus ρ.

Figure 3 plots the average BLER under the NUPS and FUPS versus M. We first observe that as M increases, the average BLER of both users decreases, indicating that employing more RIS elements can improve transmission reliability. When the NUPS is adopted, the BLER of the nerar user decreases more pronouncedly than that of the far user. In contrast, when the FUPS is adopted, the opposite is true. These results collectively

demonstrate that the network can dynamically prioritize and enhance the performance of either the near or far user by strategically allocating the reflective resources of the RIS.

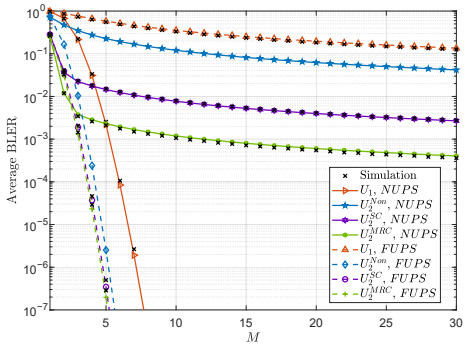


Figure 3. Average BLER under the NUPS and FUPS versus M.

Figure 4 plots the average BLER under the NUPS and FUPS versus k_1 with $M = 2$, and $k_1 = k_2$. It can be observed that as k_1 increases, the average BLER of the near and far users increases and eventually approaches 1. This inevitable convergence to an error-saturated state is fundamentally due to the distortion noise caused by hardware impairments, which imposes a finite ceiling on the achievable SNR, regardless of the transmit power. In addition, the performance gap between SC and MRC narrows as k_1 increases. This indicates that the advantage of sophisticated combining techniques diminishes under severe hardware impairments, as the system performance becomes limited by hardware-induced distortions rather than by the quality of the combined signal. Therefore, in severely impaired hardware environments, simpler techniques like SC can offer a more complexity-effective solution.

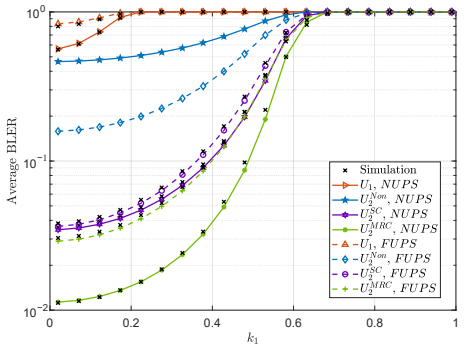


Figure 4. Average BLER under the NUPS and FUPS versus k_1 with $M = 2$, and $k_1 = k_2$.

Figure 5 plots the average BLER under the NUPS and FUPS versus Ω_{BI}. We observe that enhancing the link quality from the BS to the RIS can significantly improve the overall system reliability for all users, which demonstrates the critical role of the RIS in establishing a high-quality communication link. Moreover, it is noteworthy that the near user under the NUPS exhibits a more pronounced performance improvement with increasing Ω_{BI} compared to the near user under the FUPS. This suggests that when the RIS is deployed in close proximity to the BS, the NUPS can effectively leverage the RIS to enhance the far user's signal quality through cooperation, without sacrificing the near user's priority.

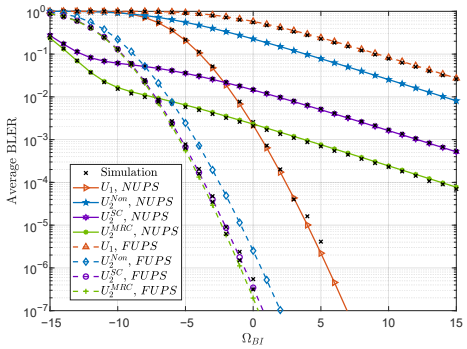


Figure 5. Average BLER under the NUPS and FUPS versus Ω_{BI}.

Figure 6 plots the average BLER under the NUPS and FUPS versus $\Omega_{U_1U_2}$ with $M = 2$, and $\alpha_1 = 0.15$. As $\Omega_{U_1U_2}$ increases, the average BLER for all cooperative schemes (SC and MRC) under the NUPS and FUPS decreases significantly. This trend confirms that a high-quality inter-user channel is crucial for enabling effective user cooperation, which is a cornerstone of the proposed system's reliability enhancement. In addition, when $\Omega_{U_1U_2}$ is small, the performance of SC for the far user reduces to the conventional non-cooperative NOMA, while it approaches the performance of MRC under large $\Omega_{U_1U_2}$. Therefore, SC demonstrates remarkable adaptability, serving as a low-complexity alternative that achieves near-optimal performance when inter-user channel conditions are favorable.

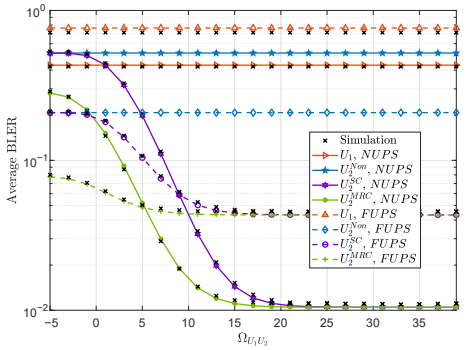


Figure 6. Average BLER under the NUPS and FUPS versus $\Omega_{U_1U_2}$ with $M = 2$, and $\alpha_1 = 0.15$.

Figure 7 plots the effective throughput under the NUPS and FUPS versus L with $M = 2$. It can be observed that an optimal blocklength exists which maximizes the effective throughput. This phenomenon arises from a fundamental trade-off in the finite blocklength regime. Specifically, shorter packets incur a higher error rate, thereby reducing the effective throughput. Conversely, longer packets introduce greater transmission latency, which can similarly degrade the overall effective throughput performance. In addition, the optimal blocklength for MRC scheme is smaller than that for SC scheme. This finding suggests that MRC is not only more reliable but also inherently better suited for latency-critical applications where shorter packets are required.

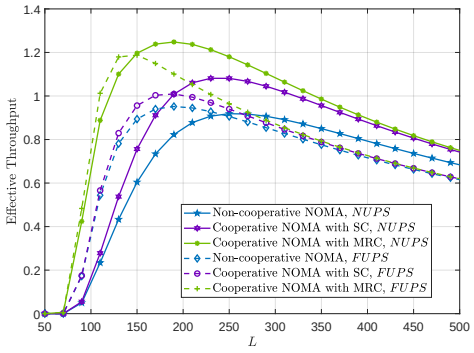


Figure 7. Effective throughput under the NUPS and FUPS versus L with $M = 2$.

Figure 8 plots the effective throughput under the NUPS and FUPS versus Ω_{BI} with $\Omega_{U_1U_2} = 5$ dB. For all schemes, the effective throughput increases significantly with improving Ω_{BI} in the low-to-medium range. This is expected, as a stronger BS-to-RIS link enhances the overall transmission reliability. However, when Ω_{BI} is high, the effective throughput for all schemes begins to saturate, as the system becomes limited by the transmission rates. In addition, cooperative NOMA schemes consistently outperform the non-cooperative NOMA, particularly in the low-to-medium Ω_{BI} region. This gain is attributed to the diversity advantage offered by cooperation, which mitigates the effects of fading and improves reliability.

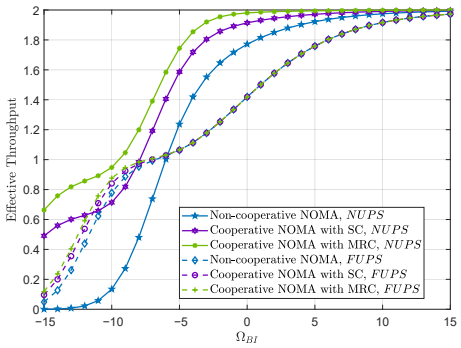


Figure 8. Effective throughput under the NUPS and FUPS versus Ω_{BI} with $\Omega_{U_1U_2} = 5$ dB.

5. Conclusions

This paper presented an investigation of the RIS-assisted cooperative NOMA network for short-packet communications in the presence of hardware impairments. To characterize the average BLER of the near and far users, closed-form expressions were derived for the NUPS and FUPS. Specifically, the analysis for the far user considered both SC and MRC reception schemes. Simulation results demonstrated that the proposed cooperative NOMA framework achieved a lower average BLER for the far user than the benchmark. In addition, when the RIS was deployed in close proximity to the BS, the NUPS effectively leveraged the RIS to enhance the far user's signal quality through cooperation without compromising the near user's priority. Moreover, SC provided a low-complexity alternative that attained near-optimal performance under favorable inter-user channel conditions. Future work can explore the integration of a STAR-RIS, which would enable unified phase-shift protocols for full-space coverage and necessitate a new performance analysis for users in the transmission and reflection regions.

Author Contributions: Formal analysis, W.S., D.C., J.L., X.Z. and Z.W.; writing—original draft preparation, W.S., D.C. and J.L.; writing—review and editing, W.S., D.C., J.L., X.Z. and Z.W.; supervision, D.C., J.L., X.Z. and Z.W. All authors have read and agreed to the published version of the manuscript.

Funding: This work was supported in part by the Key Scientific Research Projects of Colleges and Universities in Henan Province of China under Grant 23A520027 and 24A520032, in part by the Philosophy and Social Sciences Research Planning Program of Henan Province under Grant 2024ZZX024, in part by the Natural Science Foundation of Henan under Grant 252300421813, in part by the Young Backbone Teachers of Nanyang Normal University under Grant 2023-QNGG-7, and in part by the Scientific Research Project on the Development of Educational Informatization under Grant 2025KT01005.

Data Availability Statement: The data that support the findings of this study are available from the corresponding author upon reasonable request.

Acknowledgments: This article is a revised and expanded version of a paper entitled Performance Analysis of RIS-Assisted Cooperative NOMA Systems with Finite Blocklength, which was presented at the Seventeenth International Conference on Wireless Communications and Signal Processing, 2025 [44].

Conflicts of Interest: The authors declare no conflicts of interest.

Appendix A

In the NUPS, the RIS is configured to maximize the SINR for the near user. Under this configuration, the combined channel gain $\left|\mathbf{h}_{BI}^{H}\Theta\mathbf{h}_{IU_1}\right|$ can be rewritten as $\sum_{l=1}^{M}\left|h_{BI,l}\right|\left|h_{IU_1,l}\right|$. Let $G_1 = \sum_{l=1}^{M}\left|h_{BI,l}\right|\left|h_{IU_1,l}\right|$, and the first moment and the second moment of G_1 can be expressed as

$$\lambda_{G_1} = \mathbb{E}\left(\sum_{l=1}^{M}\left|h_{BI,l}\right|\left|h_{IU_1,l}\right|\right) = Mv_1, \tag{A1}$$

$$\begin{aligned}\lambda_{G_1}^{(2)} &= \mathbb{E}\left(\left(\sum_{l=1}^{M}\left|h_{BI,l}\right|\left|h_{IU_1,l}\right|\right)^2\right)\\ &= M\Omega_{BI}\Omega_{IU_1} + M(M-1)v_1^2.\end{aligned} \tag{A2}$$

Following [41], G_1 is well approximated by a Gamma distribution $G_1 \sim \Gamma(k_{G_1}, \theta_{G_1})$, where the shape and scale parameters are expressed as

$$k_{G_1} = \frac{\lambda_{G_1}^2}{\lambda_{G_1}^{(2)} - \lambda_{G_1}^2} = \frac{Mv_1^2}{\Omega_{BI}\Omega_{IU_1} - v_1^2}, \tag{A3}$$

$$\theta_{G_1} = \frac{\lambda_{G_1}}{\lambda_{G_1}^{(2)} - \lambda_{G_1}^2} = \frac{v_1}{\Omega_{BI}\Omega_{IU_1} - v_1^2}. \tag{A4}$$

After applying mathematical transformations, the CDF of G_1^2 is given by

$$F_{G_1^2}(x) = \frac{\gamma\left(k_{G_1}, \theta_{G_1}\sqrt{x}\right)}{\Gamma\left(k_{G_1}\right)}, \tag{A5}$$

and the CDF of $\gamma_{1,2}$ is given by (15).

Appendix B

From (7), the average BLER at U_1 under the NUPS is given by

$$\begin{aligned}\bar{\varepsilon}_{U_1}^{NUPS} &= \mathbb{E}\left(\varepsilon_{1,2}^{NUPS} + \left(1-\varepsilon_{1,2}^{NUPS}\right)\varepsilon_{1,1}^{NUPS}\right) \\ &\overset{(a)}{\approx} \mathbb{E}\left(\varepsilon_{1,2}^{NUPS}\right) + \mathbb{E}\left(\varepsilon_{1,1}^{NUPS}\right),\end{aligned} \tag{A6}$$

where step (a) is based on the fact of characteristically negligible error rates observed in short-packet communications systems [31]. According to (4), $\mathbb{E}\left(\varepsilon_{1,2}^{NUPS}\right)$ can be derived as

$$\mathbb{E}\left(\varepsilon_{1,2}^{NUPS}\right) = \int_0^{\infty} \vartheta\left(\gamma_{1,2}^{NUPS}\right) f_{\gamma_{1,2}^{NUPS}}(x)dx, \tag{A7}$$

where $\vartheta\left(\gamma_{1,2}^{NUPS}\right) = \begin{cases} 1, & \gamma_{1,2}^{NUPS} \le A_2 \\ \frac{1}{2} - g_2\sqrt{L}\left(\gamma_{1,2}^{NUPS} - h_2\right), & A_2 < \gamma_{1,2}^{NUPS} < B_2 \\ 0, & \gamma_{1,2}^{NUPS} \ge B_2 \end{cases}$ represents an approximation of the instantaneous BLER and $f_{\gamma_{1,2}^{NUPS}}(x)$ represents the probability density function (PDF) of $\gamma_{1,2}^{NUPS}$. Then, three specific cases are investigated to determine the closed-form expression of $\mathbb{E}\left(\varepsilon_{1,2}^{NUPS}\right)$.

Case 1: When $\frac{\alpha_2}{\alpha_1+k_1^2+k_2^2} \le A_2$, we have $\mathbb{E}\left(\varepsilon_{1,2}^{NUPS}\right) = 1$.

Case 2: When $A_2 < \frac{\alpha_2}{\alpha_1+k_1^2+k_2^2} < B_2$, $\mathbb{E}\left(\varepsilon_{1,2}^{NUPS}\right)$ can be expressed as

$$\begin{aligned}\mathbb{E}\left(\varepsilon_{1,2}^{NUPS}\right) &= \int_0^{A_2} f_{\gamma_{1,2}^{NUPS}}(x)dx + \int_{A_2}^{\frac{\alpha_2}{\alpha_1+k_1^2+k_2^2}} \left(\frac{1}{2} - g_2\sqrt{L}\left(\gamma_{1,2}^{NUPS} - h_2\right)\right) f_{\gamma_{1,2}^{NUPS}}(x)dx \\ &\overset{(b)}{=} \frac{g_2\sqrt{L}}{\Gamma\left(k_{G_1}\right)} \int_{A_2}^{\frac{\alpha_2}{\alpha_1+k_1^2+k_2^2}} \gamma\left(k_{G_1}, \theta_{G_1}\sqrt{\frac{x}{\alpha_2\rho - (\alpha_1+k_1^2+k_2^2)\rho x}}\right)dx \\ &\quad + \frac{1}{2} - g_2\sqrt{L}\left(\frac{\alpha_2}{\alpha_1+k_1^2+k_2^2} - h_2\right) \\ &\overset{(c)}{\approx} g_2\sqrt{L}\sum_{n=1}^{N} \frac{\pi\sqrt{1-t_n^2}\left(\alpha_2 - A_2\left(\alpha_1+k_1^2+k_2^2\right)\right)}{2N\Gamma\left(k_{G_1}\right)\left(\alpha_1+k_1^2+k_2^2\right)} \\ &\quad \times \gamma\left(k_{G_1}, \theta_{G_1}\sqrt{\frac{\mu_2}{\alpha_2\rho - (\alpha_1+k_1^2+k_2^2)\rho\mu_2}}\right) \\ &\quad + \frac{1}{2} - g_2\sqrt{L}\left(\frac{\alpha_2}{\alpha_1+k_1^2+k_2^2} - h_2\right),\end{aligned} \tag{A8}$$

where step (b) derives from applying partial integration and step (c) is calculated through Gaussian-Chebyshev quadrature.

Case 3: When $B_2 \le \frac{\alpha_2}{\alpha_1+k_1^2+k_2^2}$, using a similar analytical method as implemented for Case 2, $\mathbb{E}\left(\varepsilon_{1,2}^{NUPS}\right)$ can be expressed as

$$\begin{aligned}\mathbb{E}\left(\varepsilon_{1,2}^{NUPS}\right) &= g\sqrt{L}\int_{A_2}^{B_2} \frac{\gamma\left(k_{G_1}, \theta_{G_1}\sqrt{\frac{x}{\alpha_2\rho-\left(\alpha_1+k_1^2+k_2^2\right)\rho x}}\right)}{\Gamma\left(k_{G_1}\right)}dx \\ &\approx \sum_{n=1}^{N} \frac{\pi g_2\sqrt{L}(B_2-A_2)}{2N\Gamma\left(k_{G_1}\right)}\sqrt{1-t_n^2}\gamma\left(k_{G_1}, \theta_{G_1}\sqrt{\frac{\mu_1}{\alpha_2\rho - (\alpha_1+k_1^2+k_2^2)\rho\mu_1}}\right).\end{aligned} \tag{A9}$$

Combining the three aforementioned cases yields the closed-form solution for $\mathbb{E}\left(\varepsilon_{1,2}^{NUPS}\right)$, presented in (23). Following this derivation, $\mathbb{E}\left(\varepsilon_{1,1}^{NUPS}\right)$ can be obtained through an analogous methodology to that used for $\mathbb{E}\left(\varepsilon_{1,2}^{NUPS}\right)$, as demonstrated in (24).

Appendix C

According to (8), $\mathbb{E}\left(\Psi\left(\gamma_{2,2}^{1,NUPS}, b_2, L\right)\right)$ can be expressed as

$$\mathbb{E}\left(\Psi\left(\gamma_{2,2}^{1,NUPS}, b_2, L\right)\right) = \int_0^{\infty} \vartheta\left(\gamma_{2,2}^{1,NUPS}\right) f_{\gamma_{2,2}^{1,NUPS}}(x)dx. \tag{A10}$$

Then, we consider three specific cases to derive the closed-form expression for $\mathbb{E}\left(\Psi\left(\gamma_{2,2}^{1,NUPS}, b_2, L\right)\right)$.

Case 1: When $\frac{\alpha_2}{\alpha_1+k_1^2+k_2^2} \leq A_2$, we have $\mathbb{E}\left(\Psi\left(\gamma_{2,2}^{1,NUPS}, b_2, L\right)\right) = 1$.

Case 2: When $A_2 < \frac{\alpha_2}{\alpha_1+k_1^2+k_2^2} < B_2$, $\mathbb{E}\left(\Psi\left(\gamma_{2,2}^{1,NUPS}, b_2, L\right)\right)$ can be expressed as

$$\begin{aligned}
\mathbb{E}\left(\Psi\left(\gamma_{2,2}^{1,NUPS}, b_2, L\right)\right) &= \int_0^{A_2} f_{\gamma_{2,2}^{1,NUPS}}(x)dx \\
&\quad + \int_{A_2}^{\frac{\alpha_2}{\alpha_1+k_1^2+k_2^2}} \left(\frac{1}{2} - g_2\sqrt{L}\left(\gamma_{2,2}^{1,NUPS} - h_2\right)\right) f_{\gamma_{2,2}^{1,NUPS}}(x)dx \\
&= \frac{1}{2} - g_2\sqrt{L}\int_{A_2}^{\frac{\alpha_2}{\alpha_1+k_1^2+k_2^2}} e^{-\frac{x}{M\Omega_{BI}\Omega_{IU_2}\left(\alpha_2\rho-\left(\alpha_1+k_1^2+k_2^2\right)\rho x\right)}} dx \\
&\overset{(d)}{=} \frac{1}{2} - \frac{g_2\sqrt{L}\alpha_2 e^{\frac{1}{p_1}}\left(\zeta\left(A_2^1+p_1\right) - \zeta\left(\frac{1}{2p_1}+p_1\right)\right)}{p_1^2\left(\rho M\Omega_{BI}\Omega_{IU_2}\right)^{-1}},
\end{aligned} \tag{A11}$$

where step (d) is derived from [45], 3.351.4.

Case 3: When $B_2 \leq \frac{\alpha_2}{\alpha_1+k_1^2+k_2^2}$, we apply an analytical method similar to that used for Case 2 to express $\mathbb{E}\left(\Psi\left(\gamma_{2,2}^{1,NUPS}, b_2, L\right)\right)$ as

$$\begin{aligned}
\mathbb{E}\left(\Psi\left(\gamma_{2,2}^{1,NUPS}, b_2, L\right)\right) &= g_2\sqrt{L}\int_{A_2}^{B_2} 1 - e^{-\frac{x}{M\Omega_{BI}\Omega_{IU_2}\left(\alpha_2\rho-\left(\alpha_1+k_1^2+k_2^2\right)\rho x\right)}} dx \\
&= 1 - \frac{g_2\sqrt{L}\alpha_2 e^{\frac{1}{p_1}}}{p_1^2\left(\rho M\Omega_{BI}\Omega_{IU_2}\right)^{-1}}\left(\zeta\left(A_2^1+p_1\right) - \zeta\left(B_2^1+p_1\right)\right).
\end{aligned} \tag{A12}$$

The closed-form solution for $\mathbb{E}\left(\Psi\left(\gamma_{2,2}^{1,NUPS}, b_2, L\right)\right)$, which combines the three aforementioned cases, is given in (26).

References

1. Liu, Y.; Mu, X.; Liu, X.; Renzo, M.D.; Ding, Z.; Schober, R. Reconfigurable Intelligent Surface-Aided Multi-User Networks: Interplay Between NOMA and RIS. *IEEE Wirel. Commun.* **2022**, *29*, 169–176. [CrossRef]
2. Li, X.; Liu, M.; Dang, S.; Luong, N.C.; Yuen, C.; Nallanathan, A.; Niyato, D. Covert Communications with Enhanced Physical Layer Security in RIS-Assisted Cooperative Networks. *IEEE Trans. Wirel. Commun.* **2025**, *24*, 5605–5619. [CrossRef]
3. Zeng, M.; Hao, W.; Peng, Z.; Chu, Z.; Li, X.; You, C.; Pan, C. Resource Allocation for Ris-Empowered Wireless Communications: Low-Complexity and Robust Designs. *IEEE Wirel. Commun.* **2024**, *31*, 68–75. [CrossRef]
4. Yang, H.; Kim, S.; Kim, H.; Bang, S.; Kim, Y.; Kim, S.; Park, K.; Kwon, D.; Oh, J. Beyond Limitations of 5G with RIS: Field Trial in a Commercial Network, Recent Advances, and Future Directions. *IEEE Commun. Mag.* **2024**, *62*, 132–138. [CrossRef]
5. Li, X.; Zhao, J.; Chen, G.; Hao, W.; Da Costa, D.B.; Nallanathan, A.; Shin, H.; Yuen, C. TAR-RIS Assisted Covert Wireless Communications with Randomly Distributed Blockages. *IEEE Trans. Wirel. Commun.* **2025**, *24*, 4690–4705. [CrossRef]

6. Zhang, Y.; Guan, X.; Wu, Q.; Zhang, R.; Ma, Y.; Miao, C.; Wu, W.; Cai, Y. Minimize Age of Information for IRS-Aided Sensor Systems: How Many IRS Elements Are Needed? *IEEE Sens. J.* **2025**, *25*, 14099–14111. [CrossRef]
7. Li, X.; Wang, Q.; Zeng, M.; Liu, Y.; Dang, S.; Tsiftsis, T.A.; Dobre, O.A. Physical-Layer Authentication for Ambient Backscatter-Aided NOMA Symbiotic Systems. *IEEE Trans. Commun.* **2023**, *71*, 2288–2303. [CrossRef]
8. Zhang, Y.; Guan, X.; Ding, G.; Yang, W.; Yu, B.; Zhang, R.; Wu, W.; Cai, Y. Optimizing Age of Information for IRS-Assisted NOMA-Based Short Packet Communication Systems. *IEEE Trans. Cogn. Commun. Netw.* 2025, *early access*. [CrossRef]
9. Xiang, Z.; Yang, W.; Cai, Y.; Ding, Z.; Song, Y.; Zou, Y. NOMA-Assisted Secure Short-Packet Communications in IoT. *IEEE Wireless Commun.* **2020**, *27*, 8–15. [CrossRef]
10. Ding, Z.; Peng, M.; Poor, H.V. Cooperative Non-Orthogonal Multiple Access in 5G Systems. *IEEE Commun. Lett.* **2020**, *27*, 8–15. [CrossRef]
11. Dinh, P.; Arfaoui, M.A.; Sharafeddine, S.; Assi, C.M.; Ghrayeb, A. A Low-Complexity Framework for Joint User Pairing and Power Control for Cooperative NOMA in 5G and Beyond Cellular Networks. *IEEE Trans. Commun.* **2020**, *68*, 6737–6749. [CrossRef]
12. Zuo, J.; Liu, Y.; Al-Dhahir, N. Reconfigurable Intelligent Surface Assisted Cooperative Non-Orthogonal Multiple Access Systems. *IEEE Trans. Commun.* **2021**, *69*, 6750–6764. [CrossRef]
13. Fu, S.; Wang, Y.; Feng, X.; Di, B.; Li, C. Reconfigurable Intelligent Surface Assisted Non-Orthogonal Multiple Access Network Based on Machine Learning Approaches. *IEEE Netw.* **2024**, *38*, 272–279. [CrossRef]
14. Elhattab, M.; Arfaoui, M.A.; Assi, C.; Ghrayeb, A. Reconfigurable Intelligent Surface Enabled Full-Duplex/Half-Duplex Cooperative Non-Orthogonal Multiple Access. *IEEE Trans. Wirel. Commun.* **2022**, *21*, 3349–3364. [CrossRef]
15. Gu, X.; Zhang, G.; Zhuo, B.; Duan, W.; Wang, J.; Wen, M.; Ho, P.H. On the Performance of Cooperative NOMA Downlink: A RIS-Aided D2D Perspective. *IEEE Trans. Cogn. Commun. Netw.* **2023**, *9*, 1610–1624. [CrossRef]
16. Zhang, G.; Gu, X.; Duan, W.; Wen, M.; Choi, J.; Gao, F.; Ho, P. H. Hybrid Time-Switching and Power-SPlitting Relaying -Ris-Noma Downlink. *IEEE Trans. Cogn. Commun. Netw.* **2023**, *9*, 146–158. [CrossRef]
17. Ren, J.; Lei, X.; Peng, Z.; Tang, X.; Dobre, O.A. RIS-Assisted Cooperative NOMA With SWIPT. *IEEE Wirel. Commun. Lett.* **2023**, *12*, 446–450. [CrossRef]
18. Muhammad, A.; Elhattab, M.; Arfaoui, M.A.; Assi, C. Optimizing Age of Information in RIS-Empowered Uplink Cooperative NOMA Networks. *IEEE Trans. Netw. Serv. Manag.* **2024**, *21*, 897–907. [CrossRef]
19. Toregozhin, T.; Shaikh, M.; Almagambetov, A.; Nauryzbayev, G. Performance of STAR-RIS-aided cooperative NOMA networks under Nakagami-m fading. *Ad Hoc Netw.* **2024**, *156*, 103399. [CrossRef]
20. Zhang, Z.; Lung, C.-H.; Wei, X.; Chen, M.; Chatterjee, S.; Zhang, Z. In-Network Caching for ICN-Based IoT (ICN-IoT): A Comprehensive Survey. *IEEE Internet Things J.* **2023**, *10*, 14595–14620. [CrossRef]
21. Zhang, X.; Chen, M. Deep Learning Empowered Real-Time Haptic Communications for IoT. *IEEE Trans. Consum. Electron.* **2025**, *71*, 5606–5618. [CrossRef]
22. Ma, R.; Yang, W.; Guan, X.; Lu, X.; Song, Y.; Chen, D. Covert mmWave Communications with Finite Blocklength Against Spatially Random Wardens. *IEEE Internet Things J.* **2024**, *11*, 3402–3416. [CrossRef]
23. Shirvanimoghaddam, M.; Mohammadi, M.S.; Abbas, R.; Minja, A.; Yue, C.; Matuz, B.; Han, G.; Lin, Z.; Liu, W.; Li, Y.; et al. Short Block-Length Codes for Ultra-Reliable Low Latency Communications. *IEEE Commun. Mag.* **2019**, *57*, 130–137. [CrossRef]
24. Polyanskiy, Y.; Poor, H.V.; Verdu, S. Channel Coding Rate in the Finite Blocklength Regime. *IEEE Trans. Inf. Theory* **2010**, *56*, 2307–2359. [CrossRef]
25. Vu, T.-H.; Nguyen, T.-V.; Costa, D.B.d.; Kim, S. Intelligent Reflecting Surface-Aided Short-Packet Non-Orthogonal Multiple Access Systems. *IEEE Trans. Veh. Technol.* **2022**, *71*, 4500–4505. [CrossRef]
26. Yuan, L.; Du, Q.; Yang, N.; Fang, F.; Yang, N. Performance Analysis of IRS-Aided Short-Packet NOMA Systems Over Nakagami-m Fading Channels. *IEEE Trans. Veh. Technol.* **2023**, *72*, 8228–8233. [CrossRef]
27. Lou, Y.; Zou, Y.; Wang, H.; Zhai, L.; Li, Y. Joint Phase Shifts and Blocklength Resources Optimization in RIS-Assisted NOMA Short-Packet Systems. *IEEE Trans. Veh. Technol.* **2024**, *73*, 12132–12136. [CrossRef]
28. Wang, H.; Fu, Y.; Shi, Z.; Feng, Y. Joint Throughput and Blocklength Optimization for RIS-Aided Hybrid Multi-Access Short-Packet System. *IEEE Wirel. Commun. Lett.* **2024**, *13*, 2787–2791. [CrossRef]
29. Yang, J.; Zhao, L.; Ding, J.; Ding, Z. Performance Analysis of Short-Packet NOMA Systems Assisted by IRS With Failed Elements. *IEEE Trans. Veh. Technol.* **2024**, *73*, 5959–5964. [CrossRef]
30. Lioce, S.; Avitabile, G.; Florio, A.; Saucez, D.; Dabbous, W. The Impact of the Circuit Non-Idealities on the System-Level Communication Metrics in Reconfigurable Intelligent Surfaces. In Proceedings of the 2025 IEEE 16th Latin America Symposium on Circuits and Systems (LASCAS), Sao Paulo, Brazil, 25–28 February 2025.
31. Xia, C.; Xiang, Z.; Su, B.; Liu, H.; Meng, J.; Pan, G. RIS-NOMA-Assisted Short-Packet Communication with Hardware Impairments. *IEEE Internet Things J.* **2024**, *11*, 2990–3002. [CrossRef]
32. Ren, Y.; Wang, J.; Zhang, X.; Lv, T.; Lin, S.; Lu, G. RIS Assisted Short-Packet NOMA Systems with Discrete Phase Shifts and Hardware Impairments. *IEEE Internet Things J.* 2025, *early access*. [CrossRef]

33. Kumar, S.; Kumbhani, B. Wireless-Powered Reconfigurable-Intelligent-Surface-Aided Cognitive NOMA Network with Hardware Impairments: IBL and FBL Analysis. *IEEE Internet Things J.* **2025**, *12*, 17473–17486. [CrossRef]
34. Ma, R.; Li, Y.; Deng, H.; Zhang, J. Performance of RIS-Aided Short-Packet NOMA Networks with Hardware Impairments and Imperfect SIC. In Proceedings of the 2024 7th International Conference on Information Communication and Signal Processing (ICICSP), Zhoushan, China, 21–23 September 2024; pp. 253–258.
35. Kumar, S.; Kumbhani, B. Performance Analysis of Active STAR-RIS-assisted NOMA with Hardware Impairments at Finite Blocklength. *Digit. Signal Process.* **2025**, *163*, 105206. [CrossRef]
36. Zheng, J.; Wu, T.; Yao, J.; Yuen, C.; Ding, Z.; Adachi, F. Exploring the Impact of RIS on Cooperative NOMA URLLC Systems: A Theoretical Perspective. *IEEE Trans. Wirel. Commun.* 2025, *in press*. [CrossRef]
37. Yue, X.; Song, M.; Ouyang, C.; Liu, Y.; Li, T.; Hou, T. Exploiting Active RIS in NOMA Networks with Hardware Impairments. *IEEE Trans. Veh. Technol.* **2024**, *73*, 8207–8221. [CrossRef]
38. Björnson, E.; Sanguinetti, L. Rayleigh fading modeling and channel hardening for reconfigurable intelligent surfaces. *IEEE Wirel. Commun. Lett.* **2021**, *10*, 830–834. [CrossRef]
39. Wei, L.; Huang, C.; Alexandropoulos, G.C.; Yuen, C.; Zhang, Z.; Debbah, M. Channel estimation for RIS-empowered multi-user MISO wireless communications. *IEEE Trans. Commun.* **2021**, *69*, 4144–4157. [CrossRef]
40. Taha, A.; Alrabeiah, M.; Alkhateeb, A. Enabling large intelligent surfaces with compressive sensing and deep learning. *IEEE Access* **2021**, *9*, 44304–44321. [CrossRef]
41. Tahir, B.; Schwarz, S.; Rupp, M. Analysis of Uplink IRS-Assisted NOMA Under Nakagami-m Fading via Moments Matching. *IEEE Wirel. Commun. Lett.* **2021**, *10*, 624–628. [CrossRef]
42. Lai, X.; Zhang, Q.; Qin, J. Cooperative NOMA Short-Packet Communications in Flat Rayleigh Fading Channels. *IEEE Trans. Veh. Technol.* **2019**, *68*, 6182–6186. [CrossRef]
43. Vu, T.-H.; Nguyen, T.-V.; Nguyen, T.-T.; Bao, V.N.Q.; Kim, S. Short-Packet Communications in NOMA-CDRT IoT Networks with Cochannel Interference and Imperfect SIC. *IEEE Trans. Veh. Technol.* **2022**, *71*, 5552–5557. [CrossRef]
44. Song, W.; Chen, D.; Li, J.; Zhang, X.; Wang, Z. Performance Analysis of RIS-Assisted Cooperative NOMA Systems with Finite Blocklength. In Proceedings of the 2025 International Conference on Wireless Communications and Signal Processing, Chongqing, China, 23–25 October 2025.
45. Gradshteyn, I.S.; Ryzhik, I.M. *Table of Integrals Series, and Products*; Zwillinger, D., Ed.; Elsevier: New York, NY, USA, 2014.

Disclaimer/Publisher's Note: The statements, opinions and data contained in all publications are solely those of the individual author(s) and contributor(s) and not of MDPI and/or the editor(s). MDPI and/or the editor(s) disclaim responsibility for any injury to people or property resulting from any ideas, methods, instructions or products referred to in the content.